

# Exact steady states and fragmentation-induced relaxation in the no-passing asymmetric simple exclusion process

Urei Miura<sup>1,2,\*</sup>

<sup>1</sup>*Division of Physics and Astronomy, Graduate School of Science, Kyoto University, Kyoto 606-8502, Japan*

<sup>2</sup>*Center for Gravitational Physics and Quantum Information,  
Yukawa Institute for Theoretical Physics, Kyoto University,  
Kitashirakawa Oiwake-Cho, Kyoto 606-8502, Japan*

We introduce a multi-species generalization of the asymmetric simple exclusion process (ASEP) with a “no-passing” constraint, forbidding overtaking, on a one-dimensional open chain. This no-passing rule fragments the Hilbert space into an exponential number of disjoint sectors labeled by the particle sequence, leading to relaxation dynamics that depend sensitively on the initial ordering. We construct exact matrix-product steady states in every particle sequence sector and derive closed-form expressions for the particle-number distribution and two-point particle correlation functions. In the two-species case, we identify a parameter regime where some sectors relax in finite time while others exhibit metastable relaxation dynamics, revealing the coexistence of fast and slow dynamics and strong particle sequence sector dependence. Our results uncover a novel mechanism for non-equilibrium metastability arising from Hilbert space fragmentation in exclusion processes.

## I. INTRODUCTION

In the field of nonequilibrium statistical physics, the asymmetric simple exclusion process (ASEP) has long been studied as a fundamental model [1–3]. ASEP is a simple model in which particles hop randomly subject to a hard-core exclusion constraint and finds applications in phenomena ranging from traffic flow [4] to biological transport [5]. A remarkable feature of ASEP is its integrability due to an underlying quantum-group symmetry, which allows analysis via the Bethe ansatz and exact determination of steady states through the matrix product ansatz [6, 7]. Both duality relations (see Ref. [8]) and the connection to Kardar–Parisi–Zhang universality [9] have attracted considerable attention and have been investigated.

In this work, we extend the ASEP to include  $M$  species of particles and impose a “no-passing” constraint, meaning particles cannot overtake each other, drastically altering the model’s relaxation dynamics. The present model corresponds to Solution CII in the ASEP classification of Ref. [7]. Its behavior under periodic boundary conditions was examined in [10], while the open-boundary TASEP was analyzed in Ref. [11]. In this work, we focus on the ASEP with open boundaries to investigate the congestion phenomena that arise once the complete jam at the chain’s edge in TASEP is alleviated, unveiling the intricate congestion patterns that emerge. This “no-passing” model can be mapped onto a frustration-free quantum many-body system, enabling all steady states to be obtained exactly and explicitly. Similar to the Hubbard model with infinite on-site repulsion [12, 13] and  $t$ - $J_z$  model [14], the no-passing constraint leads to an exponential fragmentation of the Hilbert space into exponentially many sectors (Hilbert space fragmentation,

HSF) [15, 16]. As a result, the relaxation dynamics do not converge to a single “typical” state but remain strongly dependent on the initial condition.

The structure of this paper is as follows. In Sec. II, we introduce the multi-species no-passing ASEP, formulate its master equation, and perform the imaginary-gauge similarity transformation to obtain a Hermitian Hamiltonian. In Sec. III we detail the various symmetries of the model, including global  $U(1)$  conservation, parity, and species-swap unitaries, and the particle sequence-preserving operator responsible for Hilbert space fragmentation. In Sec. IV, we use Perron–Frobenius arguments to prove the uniqueness of the ground state in each particle sequence sector and exhibit the frustration-free nature. Sec. V constructs the exact matrix-product steady states of the non-Hermitian Markov generator, derives the normalization in closed form. In Sec. VC we develop the transfer-matrix method to compute exact one and two-point density correlations. In Sec. VI, we analyze the many-body spectral gap in the two-species system and identify three regimes: a finite-gap regime that controls fast relaxation, a gapless regime where relaxation slows down algebraically with system size and a regime in which the gap is exponentially small in system size, giving rise to metastable dynamics. Finally, Sec. VII summarizes our main findings and outlines several avenues for future work. Appendix A shows how single-species sectors reduce to the standard ASEP and map to the Ising-like ferromagnetic XXZ chain. Appendix B presents an algebraic steady state construction via quantum-group like raising operators. Appendix C provides numerical evidence for a finite bulk gap using Knabe’s method. Appendix D collects detailed scaling data for the minimal-gap sector. Appendix E gives the explicit matrix representation used in our exact diagonalization studies.

\* [urei.miura@yukawa.kyoto-u.ac.jp](mailto:urei.miura@yukawa.kyoto-u.ac.jp)

## II. MODEL: NO-PASSING ASEP

We consider a one-dimensional lattice of length  $L$  with open boundary conditions (OBC). Each site can hold at most one particle, enforcing hard-core exclusion. There are  $M$  particle species. We denote a particle of species  $\sigma \in \{1, 2, \dots, M\}$  at site  $j$  by  $|\sigma\rangle_j$ . An empty site is denoted by  $|0\rangle_j$ . A particle of species  $\sigma$  hops to a neighboring empty site, moving left with probability  $p_\sigma$  and right with probability  $1-p_\sigma$ . As a result, particles cannot overtake one another. (Fig. 1).

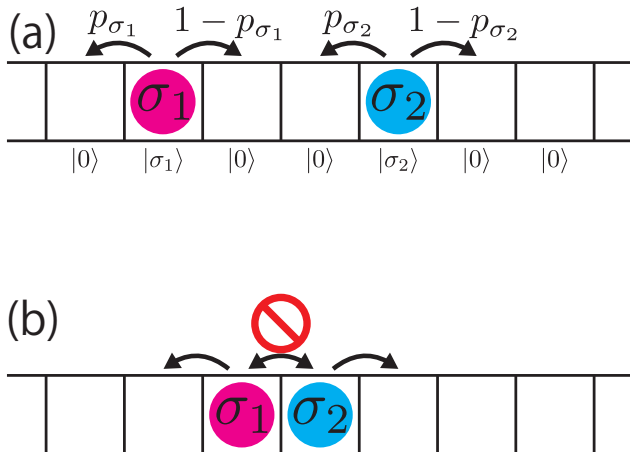


FIG. 1. Schematic of the no-passing ASEP rules. (a): A particle hops only when the adjacent site is empty. (b): Hopping into an occupied site is forbidden, so overtaking is not allowed.

This model is a special case of Solution CII in [7]. The periodic boundary condition (PBC) case was studied in [10], while the open-boundary TASEP (Totally Asymmetric Simple Exclusion Process) case was studied in [11]. In this paper, we consider the ASEP with open boundary conditions to investigate congestion phenomena that are rarely observed under periodic boundary conditions and which, in the TASEP limit, reduce to a simple boundary pile-up.

### A. Notation and Operator Definitions

We denote the vacuum state by  $|\Omega\rangle := |0, \dots, 0\rangle$ . We define the hard-core boson creation operator on each site by  $b_\sigma^\dagger := |\sigma\rangle\langle 0|$ . The hard-core condition  $b_\sigma^\dagger b_\tau^\dagger = 0$  applies for each site. We define the on-site particle number operator by  $\hat{n}_\sigma := b_\sigma^\dagger b_\sigma = |\sigma\rangle\langle\sigma|$ . We define the on-site total particle number operator by  $\hat{n} := \sum_{\sigma=1}^M \hat{n}_\sigma = 1 - |0\rangle\langle 0|$ . These operators are projectors with eigenvalues 0 or 1. We use the index  $\mu = 0, 1, \dots, M$  to label the states  $|\mu\rangle$ , including the empty state ( $\mu = 0$ ) and the

particle states ( $\mu \geq 1$ ). For each  $p_\sigma$ , we define

$$q_\sigma := \sqrt{\frac{1-p_\sigma}{p_\sigma}}, \quad (1)$$

and shown in Fig. 2 is the relation  $p_\sigma$  and  $q_\sigma$ .

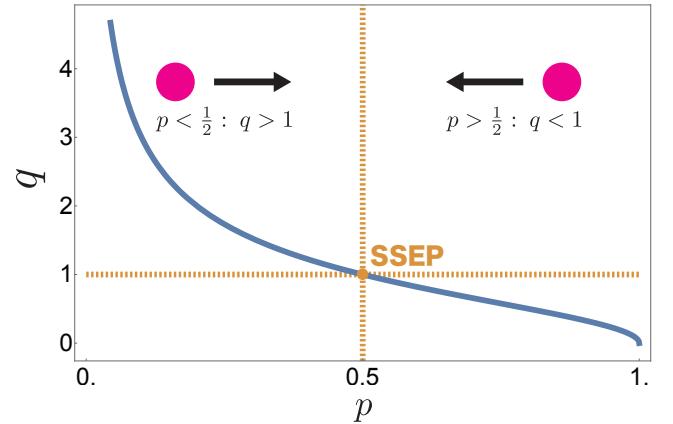


FIG. 2. Relation between  $p$  and  $q$ . For  $0 < p < 1/2$ , the bias is to the right ( $q > 1$ ). For  $1/2 < p < 1$ , the bias is to the left ( $q < 1$ ). At  $p = 1/2$  (symmetric simple exclusion process, SSEP case),  $q = 1$ .

### B. Master Equation

We represent the continuous-time Markov process by the probability vector  $|P(t)\rangle$ . The master equation reads

$$\frac{d}{dt} |P(t)\rangle = -\tilde{H} |P(t)\rangle. \quad (2)$$

Here,  $-\tilde{H}$  is the generally non-Hermitian transition matrix of the continuous time Markov process. The probability of configuration  $\{\mu\}$ , corresponding to  $|\{\mu\}\rangle = |\mu_1, \dots, \mu_L\rangle$ , is

$$P(\{\mu\}; t) = \langle\{\mu\}|P(t)\rangle. \quad (3)$$

Normalization of the probability vector is

$$\begin{aligned} 1 &= \sum_{\{\mu\}} P(\{\mu\}; t) \\ &= \sum_{\{\mu\}} \langle\{\mu\}|P(t)\rangle. \end{aligned} \quad (4)$$

We treat  $\tilde{H}$  as a non-Hermitian Hamiltonian. We enumerate all its zero-energy ground states, which correspond to the steady state of the Markov process. Because  $\tilde{H}$  is a transition matrix, its eigenvalues have non-negative real parts. Each connected component has one zero-energy steady state by the Perron-Frobenius theorem. For  $M = 2$ , we also study the energy gap as an estimate of the relaxation time to the steady state.

The operator  $\tilde{H}$  encodes the processes  $|0, \sigma\rangle \rightarrow |\sigma, 0\rangle : p_\sigma$ ,  $|\sigma, 0\rangle \rightarrow |0, \sigma\rangle : 1 - p_\sigma$ , and  $|\sigma_1, \sigma_2\rangle \rightarrow |\sigma_2, \sigma_1\rangle : 0$  (see Fig. 1). We define

$$\begin{aligned} \tilde{H} &= \sum_{j=1}^{L-1} \tilde{h}_{j,j+1}, \\ \tilde{h}_{j,j+1} &= \\ &- \sum_{\sigma=1}^M \left[ p_\sigma b_{j,\sigma}^\dagger b_{j+1,\sigma} + (1 - p_\sigma) b_{j+1,\sigma}^\dagger b_{j,\sigma} \right] \\ &+ \sum_{\sigma=1}^M \left[ p_\sigma (1 - \hat{n}_j) \hat{n}_{j+1,\sigma} + (1 - p_\sigma) \hat{n}_{j,\sigma} (1 - \hat{n}_{j+1}) \right]. \end{aligned} \quad (5)$$

Throughout this paper, we consider the ASEP (i.e.  $0 < p_\sigma < 1$ ) under open boundary conditions (OBC), and do not take the TASEP limit.

### C. Similarity Transformation to a Hermitian Hamiltonian

For  $0 < p_\sigma < 1$ , the non-Hermitian operator  $\tilde{H}$  can be transformed by the invertible but nonunitary operator

$$\begin{aligned} S &:= \prod_{\sigma=1}^M S_\sigma, \quad S_\sigma := q_\sigma^{-\sum_{j=1}^L j \hat{n}_{j,\sigma}}, \\ S^{-1} &= \prod_{j=1}^L \left[ (1 - \hat{n}_j) + \sum_{\sigma=1}^M q_\sigma^j \hat{n}_{j,\sigma} \right], \end{aligned} \quad (6)$$

into the Hermitian Hamiltonian

$$\begin{aligned} H &:= S \tilde{H} S^{-1} = \sum_{j=1}^{L-1} h_{j,j+1}, \\ h_{j,j+1} &= \\ &- \sum_{\sigma=1}^M \sqrt{p_\sigma (1 - p_\sigma)} \left( b_{j,\sigma}^\dagger b_{j+1,\sigma} + b_{j+1,\sigma}^\dagger b_{j,\sigma} \right) \\ &+ \sum_{\sigma=1}^M \left[ p_\sigma (1 - \hat{n}_j) \hat{n}_{j+1,\sigma} + (1 - p_\sigma) \hat{n}_{j,\sigma} (1 - \hat{n}_{j+1}) \right]. \end{aligned} \quad (7)$$

This extends the known Hermitianization for single-species ASEP under OBC [17]. In non-Hermitian physics, it is known as the Hatano–Nelson pure imaginary gauge transformation with OBC [18, 19]. Because similarity transformations preserve the spectrum,  $H$  has a real spectrum under OBC. If  $|\Psi\rangle$  is an eigenstate of  $H$ , then the corresponding probability eigenvector for  $\tilde{H}$  is

$$|P\rangle = S^{-1} |\Psi\rangle. \quad (8)$$

Their relation is illustrated by:

$$\begin{array}{ccc} \tilde{H} & \xrightarrow{S} & H := S \tilde{H} S^{-1} \\ \text{eigenstate} \downarrow & & \downarrow \text{eigenstate} \\ |P\rangle = S^{-1} |\Psi\rangle & \xleftarrow{S^{-1}} & |\Psi\rangle. \end{array}$$

## III. SYMMETRIES AND UNITARY TRANSFORMATIONS

In this section, we list the symmetries of  $\tilde{H}$  and  $H$  and discuss symmetries in parameter space. We treat the sequence operator  $\mathcal{S}$  separately because it is crucial for enumerating exact ground states.

### A. Global $U(1)^{\times M}$ Symmetry

The model has a  $U(1)^{\times M}$  symmetry, which conserves the particle number of each species. Under independent phase rotations  $b_{j,\sigma} \mapsto e^{i\theta_\sigma} b_{j,\sigma}$  ( $\theta_\sigma \in \mathbb{R}$ ), both  $\tilde{H}$  and  $H$  remain invariant. Hence, each species' particle number  $\hat{N}_\sigma := \sum_{j=1}^L \hat{n}_{j,\sigma}$  is conserved:

$$[\tilde{H}, \hat{N}_\sigma] = [H, \hat{N}_\sigma] = 0. \quad (9)$$

Consequently, the total particle number  $\hat{N} := \sum_{j=1}^L \hat{n}_j$  is conserved as well.

### B. Parity and Species-Swap Unitaries

We define the parity unitary transformation that swaps left and right on the lattice by:

$$P^\dagger b_{j,\sigma} P = b_{L+1-j,\sigma}. \quad (10)$$

Under this transformation, the spectrum is preserved and the Hamiltonian transforms as

$$P^\dagger H(p_1, \dots, p_M) P = H(1 - p_1, \dots, 1 - p_M), \quad (11)$$

as shown in Fig. 3. Thus,  $H(p_1, \dots, p_M)$  and  $H(1 - p_1, \dots, 1 - p_M)$  have the same spectrum.

For  $1 \leq \sigma_1 < \sigma_2 \leq M$ , we define a unitary operator:

$$U_{\sigma_1, \sigma_2} := \exp \left[ i \frac{\pi}{2} \sum_{j=1}^L \left( -i b_{j,\sigma_1}^\dagger b_{j,\sigma_2} + i b_{j,\sigma_2}^\dagger b_{j,\sigma_1} \right) \right]. \quad (12)$$

This operator acts on the hard-core boson operators as

$$\begin{aligned} U_{\sigma_1, \sigma_2}^\dagger b_{j,\sigma_1} U_{\sigma_1, \sigma_2} &= b_{j,\sigma_2}, \\ U_{\sigma_1, \sigma_2}^\dagger b_{j,\sigma_2} U_{\sigma_1, \sigma_2} &= -b_{j,\sigma_1}, \end{aligned} \quad (13)$$

and it swaps  $p_{\sigma_1}$  and  $p_{\sigma_2}$  in the Hamiltonian:

$$\begin{aligned} U_{\sigma_1, \sigma_2}^\dagger H(\dots, p_{\sigma_1}, \dots, p_{\sigma_2}, \dots) U_{\sigma_1, \sigma_2} \\ = H(\dots, p_{\sigma_2}, \dots, p_{\sigma_1}, \dots). \end{aligned} \quad (14)$$

(11) and (13) imply that it suffices to study the spectrum within the simplex

$$\left\{ (p_1, \dots, p_M) \in (0, 1)^{\times M} \mid p_1 \leq \dots \leq p_M, p_1 + p_M \leq 1 \right\}. \quad (15)$$

In the following sections, when we treat the concrete examples, we focus on the  $M = 2$  case and restrict our analysis to the yellow region in Fig. 3.

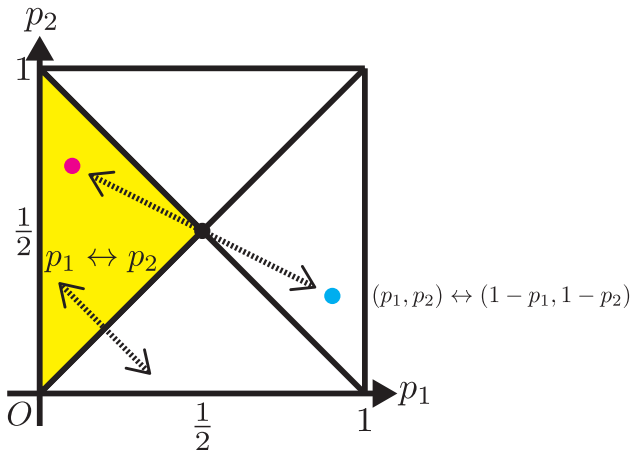


FIG. 3. Parameter relations that give the same spectrum under unitary transformations for  $M = 2$ . These relations imply that studying the spectrum in the yellow isosceles triangle is sufficient.

### C. Particle Sequence Conservation and Hilbert Space Fragmentation

The continuous time Markov dynamics generated by  $\tilde{H}$  forbids particle overtaking. Therefore, the sequence of particles  $\{\sigma\}_s = \{\sigma_1, \dots, \sigma_N\}$  is preserved. To formalize this, we introduce the sequence operator:

$$\mathcal{S} := \sum_{j=1}^L M^{\hat{n}_1 + \dots + \hat{n}_{j-1}} \sum_{\sigma=1}^M \sigma \hat{n}_{j,\sigma}. \quad (16)$$

This operator commutes with both  $H$  and  $\tilde{H}$ :

$$[H, \mathcal{S}] = [\tilde{H}, \mathcal{S}] = 0. \quad (17)$$

It has  $\sum_{k=0}^L M^k = \frac{M^{L+1}-1}{M-1}$  distinct eigenvalues. Each configuration  $\{\sigma\}_s$  maps to a unique base- $M$  eigenvalue. For example, for  $M = 2$  and  $N = 0, 1, 2$ , the eigenvalues are:

$$\begin{aligned} 0 &: |\Omega\rangle, \\ 1 &: b_{j,1}^\dagger |\Omega\rangle \quad (1 \leq j \leq L), \\ 2 &: b_{j,2}^\dagger |\Omega\rangle \quad (1 \leq j \leq L), \\ 3 &: b_{j_1,1}^\dagger b_{j_2,1}^\dagger |\Omega\rangle \quad (1 \leq j_1 < j_2 \leq L), \\ 4 &: b_{j_1,2}^\dagger b_{j_2,1}^\dagger |\Omega\rangle \quad (1 \leq j_1 < j_2 \leq L), \\ 5 &: b_{j_1,1}^\dagger b_{j_2,2}^\dagger |\Omega\rangle \quad (1 \leq j_1 < j_2 \leq L), \\ 6 &: b_{j_1,2}^\dagger b_{j_2,2}^\dagger |\Omega\rangle \quad (1 \leq j_1 < j_2 \leq L). \end{aligned} \quad (18)$$

Hence,  $H$  is block diagonal in  $\mathcal{S}$ :

$$H = \bigoplus_{\{\sigma\}_s} H^{\{\sigma\}_s} = \bigoplus_{s=0}^{\frac{M^{L+1}-1}{M-1}-1} H^{S=s}. \quad (19)$$

Here,  $H^{\{\sigma\}_s}$  and  $H^{S=s}$  are the blocks corresponding to the particle sequence  $\{\sigma\}_s$  and the eigenvalue  $s$ , respectively. This fragmentation into exponentially many sectors leads to Hilbert space fragmentation (HSF) and consequently violates the eigenstate thermalization hypothesis (ETH)[15, 16, 20]. This type of HSF due to forbidden overtaking resembles that in the Hubbard model with infinite on-site repulsion [12, 13] and the  $t$ - $J_z$  model [14].

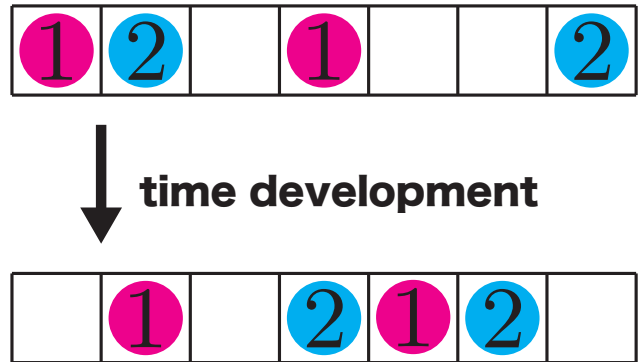


FIG. 4. Example time evolution for  $\{\sigma\}_s = \{1, 2, 1, 2\}$ . Particles can only move without changing the particle sequence  $\{1, 2, 1, 2\}$ . The motion is highly constrained in the full  $3^L$ -dimensional Hilbert space.

In Sec. IV, we use the Perron–Frobenius theorem to show that each of the  $\frac{M^{L+1}-1}{M-1}$  sectors has a unique ground state. We then show that these ground states exhaust all ground states of  $H$  and are exactly given by the form of matrix product state (MPS). Although similar to the matrix product ansatz reviewed in [7], here the bond dimension is exactly  $N + 1$  for a system with  $N$  particles and remains finite for finite  $N$ .

### D. Enhanced Symmetry in the Isotropic Limit

When  $p_1 = \dots = p_M$ ,  $H$  acquires an additional high symmetry. It commutes with the local operators  $b_{j,\sigma}^\dagger b_{j,\tau}$  for any  $j$  and any  $\sigma \neq \tau$ . This reflects that, under isotropic hopping, particle species become indistinguishable. Any eigenstate that contains particles of more than one species can be converted into some eigenstates containing only a single particle species without changing its energy by applying  $b_{j,\sigma}^\dagger b_{j,\tau}$ . Combined with the discussion in Appendix. A, this implies the spectrum (up to degeneracy) matches that of the standard ASEP.

#### IV. EXACT GROUND STATES OF “QUANTUM” HAMILTONIAN $H$

In this section, we consider the Hermitian Hamiltonian (7) as a quantum system. This is because the similarity transformation  $S$  establishes a one-to-one correspondence between the eigenvalues and eigenvectors of  $\tilde{H}$  and  $H$  so that the steady state of  $\tilde{H}$  is obtained by applying the transformation  $S^{-1}$  to the ground states of  $H$  (see Sub-Sec. IIC). Moreover,  $H$  is frustration-free, which makes its ground states readily analyzable via matrix product state (MPS) methods known in one-dimensional quantum systems. We determine the number of ground states and derive their explicit forms. By the Perron–Frobenius theorem, each sector labeled by the eigenvalue of the particle sequence operator  $\mathcal{S}$  has a unique ground state. Moreover, each ground state admits the MPS representation with the bond dimension equal to the particle number plus one.

##### A. Perron–Frobenius Proof of Ground-State Uniqueness in Each particle sequence Sector

Let  $H^{S=s}$  be the restriction of  $H$  to the sector with  $\mathcal{S} = s$  ( $s = 0, 1, \dots, \frac{M^{L+1}-1}{M-1} - 1$ ). This operator has matrix elements labeled by  $(i_1, \dots, i_N; j_1, \dots, j_N)$ :

$$H_{i_1, \dots, i_N; j_1, \dots, j_N}^{S=s} = \langle \Omega | b_{i_N, \sigma_N} \cdots b_{i_1, \sigma_1} H b_{j_1, \sigma_1}^\dagger \cdots b_{j_N, \sigma_N}^\dagger | \Omega \rangle, \quad (20)$$

with  $1 \leq i_1 < \dots < i_N \leq L$  and  $1 \leq j_1 < \dots < j_N \leq L$ . To apply the Perron–Frobenius theorem, we require connectivity of this matrix and nonpositive off-diagonal entries. Connectivity holds because any configuration can reach any other by moving particles to the left or right boundary. Nonpositivity holds since each hopping term in  $H$  has coefficient  $-\sqrt{p_\sigma(1-p_\sigma)} < 0$ . Thus each  $H^{S=s}$  satisfies the Perron–Frobenius conditions. Each sector has a unique ground state, giving  $\frac{M^{L+1}-1}{M-1}$ -fold degeneracy.

##### B. Local Projector Form and Frustration-Free Nature

We define the normalized two-site state

$$\begin{aligned} |Q_-(\sigma)\rangle &:= \sqrt{1-p_\sigma} |\sigma, 0\rangle - \sqrt{p_\sigma} |0, \sigma\rangle \\ &= \sqrt{p_\sigma} (q_\sigma |\sigma, 0\rangle - |0, \sigma\rangle). \end{aligned} \quad (21)$$

Then each two-site term of the Hamiltonian (7) can be written as

$$h_{j,j+1} = \sum_{\sigma=1}^M |Q_-(\sigma)\rangle \langle Q_-(\sigma)|_{j,j+1}. \quad (22)$$

Hence  $H$  is a sum of projectors. The product ground states  $|\Omega\rangle$  and  $|\sigma_1, \dots, \sigma_L\rangle$  confirm that  $H$  is frustration-free.

We define

$$\begin{aligned} |Q_+(\sigma)\rangle &:= \sqrt{p_\sigma} |\sigma, 0\rangle + \sqrt{1-p_\sigma} |0, \sigma\rangle \\ &= \sqrt{p_\sigma} (|\sigma, 0\rangle + q_\sigma |0, \sigma\rangle). \end{aligned} \quad (23)$$

Then, the eigensystem of  $h_{j,j+1}$  is:

$$\begin{aligned} E = 0 : \\ &|0, 0\rangle, \\ &|Q_+(\sigma)\rangle \quad (\sigma = 1, \dots, M), \\ &|\sigma_1, \sigma_2\rangle \quad (\sigma_1, \sigma_2 = 1, \dots, M), \\ E = 1 : \\ &|Q_-(\sigma)\rangle \quad (\sigma = 1, \dots, M), \end{aligned} \quad (24)$$

in total  $(M+1)^2$  states. From this, zero-energy ground states of the full system can be built as MPS.

##### C. Exact MPS Representation of ground states

Let  $N$  be the particle number. On each site, define  $(N+1) \times (N+1)$  matrices  $A$ . Before that, we define the following:

$$\lambda_m := \begin{cases} (q_{\sigma_m} \cdots q_{\sigma_N})^2, & m = 1, \dots, N, \\ 1, & m = N+1. \end{cases} \quad (25)$$

Then we set

$$A := \begin{pmatrix} \sqrt{\lambda_1} |0\rangle & & & & \\ & |\sigma_1\rangle & & & \\ & \sqrt{\lambda_2} |0\rangle & |\sigma_2\rangle & & \\ & & \ddots & \ddots & \\ & & & \sqrt{\lambda_N} |0\rangle & |\sigma_N\rangle \\ & & & & \sqrt{\lambda_{N+1}} |0\rangle \end{pmatrix}. \quad (26)$$

We also define

$$|\bar{Q}_+(\sigma)\rangle := |\sigma, 0\rangle + q_\sigma |0, \sigma\rangle. \quad (27)$$

Then for two sites, we have:



The stochastic transfer matrix is defined as

$$\begin{aligned} \tilde{\mathbf{B}} &:= \begin{array}{c} \boxed{\mathbf{M}} \\ | \\ \boxed{\mathbf{B}} \end{array} = \sum_{\mu} \langle \mu | \mathbf{B} \\ &= \begin{pmatrix} \lambda_1 & 1 & & & \\ & \lambda_2 & 1 & & \\ & & \ddots & \ddots & \\ & & & \lambda_N & 1 \\ & & & & \lambda_{N+1} \end{pmatrix}, \end{aligned} \quad (34)$$

where  $\mathbf{M} := \sum_{\mu=0}^M \langle \mu |$ . Then

$$\begin{aligned} \mathcal{N} &= \begin{array}{c} \boxed{\mathbf{M}_1} \quad \boxed{\mathbf{M}_L} \\ | \quad | \\ \boxed{\mathbf{e}_1^\top} - \boxed{\mathbf{B}_1} - \dots - \boxed{\mathbf{B}_L} - \boxed{\mathbf{e}_{N+1}} \end{array} \\ &= \mathbf{e}_1^\top \tilde{\mathbf{B}}^L \mathbf{e}_{N+1} \\ &= (\tilde{\mathbf{B}}^n)_{1,N+1}. \end{aligned} \quad (35)$$

By induction one shows for  $\forall n \in \mathbb{Z}_{\geq 0}$ ,

$$(\tilde{\mathbf{B}}^n)_{i,j} = \begin{cases} 0, & i > j, \\ \sum_{l=i}^j \frac{\lambda_l^n}{\prod_{\substack{i \leq l' \leq j \\ l' \neq l}} (\lambda_l - \lambda_{l'})}, & i \leq j. \end{cases} \quad (36)$$

Hence

$$\mathcal{N} = \sum_{l=1}^{N+1} \frac{\lambda_l^L}{\prod_{\substack{1 \leq l' \leq N+1 \\ l' \neq l}} (\lambda_l - \lambda_{l'})}. \quad (37)$$

If two eigenvalues coincide, one has to take the appropriate limit in this formula. The normalized steady state is

$$\begin{aligned} &|P_{\text{s.s.}}\rangle \\ &= \frac{\mathbf{e}_1^\top \mathbf{B}_1 \dots \mathbf{B}_L \mathbf{e}_{N+1}}{\mathcal{N}} \\ &= \frac{\begin{array}{c} | \\ \boxed{\mathbf{e}_1^\top} - \boxed{\mathbf{B}_1} - \dots - \boxed{\mathbf{B}_L} - \boxed{\mathbf{e}_{N+1}} \\ | \end{array}}{\begin{array}{c} \boxed{\mathbf{M}_1} \quad \boxed{\mathbf{M}_L} \\ | \quad | \\ \boxed{\mathbf{e}_1^\top} - \boxed{\mathbf{B}_1} - \dots - \boxed{\mathbf{B}_L} - \boxed{\mathbf{e}_{N+1}} \end{array}} \\ &= \frac{\sum_{1 \leq j_1 < \dots < j_N \leq L} q_{\sigma_1}^{2j_1-1} \dots q_{\sigma_N}^{2j_N-N} b_{j_1, \sigma_1}^\dagger \dots b_{j_N, \sigma_N}^\dagger |\Omega\rangle}{\sum_{l=1}^{N+1} \frac{\lambda_l^L}{\prod_{\substack{1 \leq l' \leq N+1 \\ l' \neq l}} (\lambda_l - \lambda_{l'})}}. \end{aligned} \quad (38)$$

### C. Particle Distribution and Correlation via Transfer-Matrix Method

The stochastic expectation of an observable  $A$  is

$$\langle A \rangle = \sum_{\{\mu\}} \langle \{\mu\} | A | P_{\text{s.s.}} \rangle. \quad (39)$$

If  $A$  is an MPO (Matrix Product Operator), one can use the transfer matrix method to compute  $\langle A \rangle$ .

#### 1. Exact Expression for $\langle \hat{n}_j \rangle$

We define

$$\begin{aligned} \tilde{\mathbf{N}} &:= \begin{array}{c} \boxed{\mathbf{M}} \\ | \\ \boxed{\hat{n}} \\ | \\ \boxed{\mathbf{B}} \end{array} = \sum_{\mu} \langle \mu | \hat{n} \mathbf{B} \\ &= \begin{pmatrix} 0 & 1 & & & \\ & 0 & 1 & & \\ & & \ddots & \ddots & \\ & & & 0 & 1 \end{pmatrix}. \end{aligned} \quad (40)$$

Then the density at site  $j$  is

$$\langle \hat{n}_j \rangle = \sum_{\{\mu\}} \langle \{\mu\} | \hat{n}_j | P_{\text{s.s.}} \rangle$$

$$\begin{aligned} &\begin{array}{c} \boxed{\mathbf{M}_1} \quad \boxed{\mathbf{M}_i} \quad \boxed{\mathbf{M}_L} \\ | \quad | \quad | \\ \boxed{\mathbf{e}_1^\top} - \boxed{\mathbf{B}_1} - \dots - \boxed{\hat{n}_j} - \dots - \boxed{\mathbf{B}_L} - \boxed{\mathbf{e}_{N+1}} \end{array} \\ &= \frac{\begin{array}{c} \boxed{\mathbf{M}_1} \quad \boxed{\mathbf{M}_L} \\ | \quad | \\ \boxed{\mathbf{e}_1^\top} - \boxed{\mathbf{B}_1} - \dots - \boxed{\mathbf{B}_L} - \boxed{\mathbf{e}_{N+1}} \end{array}}{\mathcal{N}} \\ &= \frac{\mathbf{e}_1^\top \tilde{\mathbf{B}}^{j-1} \tilde{\mathbf{N}} \tilde{\mathbf{B}}^{L-j} \mathbf{e}_{N+1}}{\mathcal{N}}. \end{aligned} \quad (41)$$

Since

$$\tilde{\mathbf{N}} = \sum_{m=1}^N \mathbf{e}_m \mathbf{e}_{m+1}^\top, \quad (42)$$

we get

$$\begin{aligned} \langle \hat{n}_j \rangle &= \sum_{m=1}^N \frac{\mathbf{e}_1^\top \tilde{\mathbf{B}}^{j-1} \mathbf{e}_m \mathbf{e}_{m+1}^\top \tilde{\mathbf{B}}^{L-j} \mathbf{e}_{N+1}}{\mathcal{N}} \\ &= \sum_{m=1}^N \frac{(\tilde{\mathbf{B}}^{j-1})_{1,m} (\tilde{\mathbf{B}}^{L-j})_{m+1,N+1}}{(\tilde{\mathbf{B}}^L)_{1,N+1}}. \end{aligned} \quad (43)$$

Using (36), this becomes

$$\langle \hat{n}_j \rangle = \sum_{m=1}^N \frac{\left( \sum_{l=1}^m \frac{\lambda_l^{j-1}}{\prod_{\substack{1 \leq l' \leq m \\ l' \neq l}} (\lambda_l - \lambda_{l'})} \right) \left( \sum_{l=m+1}^{N+1} \frac{\lambda_l^{L-j}}{\prod_{\substack{m+1 \leq l' \leq N+1 \\ l' \neq l}} (\lambda_l - \lambda_{l'})} \right)}{\sum_{l=1}^{N+1} \frac{\lambda_l^L}{\prod_{\substack{1 \leq l' \leq N+1 \\ l' \neq l}} (\lambda_l - \lambda_{l'})}}. \quad (44)$$

## 2. Exact Expression for $\langle \hat{n}_i \hat{n}_j \rangle$

The two-point correlation function  $\langle \hat{n}_i \hat{n}_j \rangle$  for  $i < j$  can be expressed using the MPS transfer matrix as

$$\begin{aligned} \langle \hat{n}_i \hat{n}_j \rangle &= \sum_{\{\mu\}} \langle \{\mu\} | \hat{n}_i \hat{n}_j | P_{\text{s.s.}} \rangle \\ &= \frac{\begin{array}{c} \boxed{M_1} \quad \boxed{M_i} \quad \boxed{M_j} \quad \boxed{M_L} \\ | \quad | \quad | \quad | \\ \boxed{e_1^\top} \boxed{B_1} \cdots \boxed{B_i} \cdots \boxed{B_j} \cdots \boxed{B_L} \boxed{e_{N+1}} \end{array}}{\begin{array}{c} \boxed{M_1} \quad \boxed{M_L} \\ | \quad | \\ \boxed{e_1^\top} \boxed{B_1} \cdots \boxed{B_L} \boxed{e_{N+1}} \end{array}} \\ &= \frac{e_1^\top \tilde{B}^{i-1} \tilde{N} \tilde{B}^{j-i-1} \tilde{N} \tilde{B}^{L-j} e_{N+1}}{\mathcal{N}} \\ &= \sum_{m_i, m_j=1}^N \frac{e_1^\top \tilde{B}^{i-1} e_{m_i} e_{m_i+1}^\top \tilde{B}^{j-i-1} e_{m_j} e_{m_j+1}^\top \tilde{B}^{L-j} e_{N+1}}{\mathcal{N}} \\ &= \sum_{m_i, m_j=1}^N \frac{(\tilde{B}^{i-1})_{1, m_i} (\tilde{B}^{j-i-1})_{m_i+1, m_j} (\tilde{B}^{L-j})_{m_j+1, N+1}}{(\tilde{B}^L)_{1, N+1}} \\ &= \sum_{1 \leq m_i < m_j \leq N} \frac{\left( \sum_{l=1}^{m_i} \frac{\lambda_l^{i-1}}{\prod_{\substack{1 \leq l' \leq m_i \\ l' \neq l}} (\lambda_l - \lambda_{l'})} \right) \left( \sum_{l=m_i+1}^{m_j} \frac{\lambda_l^{j-i-1}}{\prod_{\substack{m_i+1 \leq l' \leq m_j \\ l' \neq l}} (\lambda_l - \lambda_{l'})} \right) \left( \sum_{l=m_j+1}^{N+1} \frac{\lambda_l^{L-j}}{\prod_{\substack{m_j+1 \leq l' \leq N+1 \\ l' \neq l}} (\lambda_l - \lambda_{l'})} \right)}{\sum_{l=1}^{N+1} \frac{\lambda_l^L}{\prod_{\substack{1 \leq l' \leq N+1 \\ l' \neq l}} (\lambda_l - \lambda_{l'})}}. \quad (45) \end{aligned}$$

Here we used (36) to derive the final line.

## D. Many-Body Particle Distribution and Correlations in the Two Species Case

In this subsection, we consider the case of two particle species ( $M = 2$ ). We use the (41) and (45) derived in SubSec. V C. We calculate the steady par-

ticle number expectation  $\langle \hat{n}_j \rangle$ , the variance  $\langle \hat{n}_j^2 \rangle - \langle \hat{n}_j \rangle^2 = \langle \hat{n}_j \rangle (1 - \langle \hat{n}_j \rangle)$  ( $\hat{n}_j^2 = \hat{n}_j$ ), the correlation function  $\langle \hat{n}_i \hat{n}_j \rangle$ , and the covariance  $\langle \hat{n}_i \hat{n}_j \rangle - \langle \hat{n}_i \rangle \langle \hat{n}_j \rangle$ . We discuss how this behavior differs from that of the standard ASEP.



1.  $\langle \hat{n}_j \rangle$  and its variance in the two species case

Fig. 5 shows the particle number expectation and variance for a steady state  $|P_{s.s.}\rangle$  under the settings given in the caption. Note that since  $0 \leq \langle \hat{n}_j \rangle \leq 1$ , the variance ranges from 0 to  $\frac{1}{4}$ .

Fig. 5 (a) shows the case where both species hop preferentially to the right. Here, the particle number distribution forms a right-biased domain wall, just as in the standard ASEP. The variance is very small except at the domain-wall interface, indicating that the steady state has little nonlocal correlation. This can also be inferred from the MPS expansion in Eq. (38): since both  $q_1$  and  $q_2$  exceed 1, configurations biased to the right have exponentially larger weights, making the state close to a product state. Such behavior also appears in the OBC ASEP or the kink boundary condition XXZ model [21], so it does not differ significantly from the standard ASEP.

Fig. 5 (b) shows the case where species  $\sigma = 1$  hops preferentially to the right and species  $\sigma = 2$  hops preferentially to the left. In this case, the particle number distribution exhibits a more complex landscape, markedly different from the standard ASEP. In particular, wide regions do not saturate at  $\langle \hat{n}_j \rangle = 0$  or 1, leading to nonzero variance. This indicates that the steady state is far from a product state and has nonlocal correlations. Indeed, large regions have variance close to the maximum  $\frac{1}{4}$ . This too follows from (38), where  $q_1(> 1)$  and  $q_2(< 1)$  partially cancel among the coefficients of  $|P_{s.s.}\rangle$  obtained by expanding in the real-space basis, giving similar weights to many configurations and moving the steady state away from a product form.

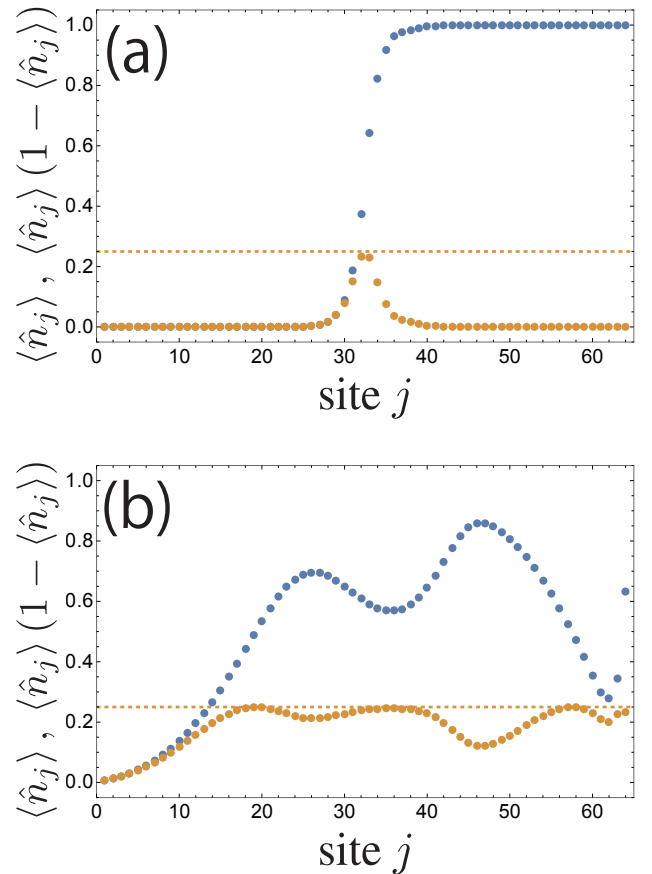


FIG. 5. Particle number expectation  $\langle \hat{n}_j \rangle$  (blue) and variance  $\langle \hat{n}_j \rangle (1 - \langle \hat{n}_j \rangle)$  (orange) for the two-species case ( $M = 2$ ), with system size  $L = 64$  and total particle number  $N = 32$ . The particle sequence is fixed as  $\{1, 1, 1, 1, 2, 2, 2, 1, 2, 2, 2, 1, 2, 2, 1, 1, 1, 2, 1, 2, 1, 2, 2, 1, 2, 2, 2, 1, 2, 2, 2, 1\}$ . (a): Both species hop preferentially to the right ( $q_1 = 1.5 > 1, q_2 = 1.25 > 1$ ), producing a simple domain-wall structure typical of standard ASEP. (b): Species 1 hops rightward ( $q_1 = 1.5 > 1$ ) and species 2 hops leftward ( $q_2 = 0.75 < 1$ ), creating a more complex and strongly correlated density profile absent in standard ASEP.

2.  $\langle \hat{n}_i \hat{n}_j \rangle$  and its cumulant in the two species case

Fig. 6 and Fig. 7 display color plots of the correlation function  $\langle \hat{n}_i \hat{n}_j \rangle$  and its cumulant  $\langle \hat{n}_i \hat{n}_j \rangle - \langle \hat{n}_i \rangle \langle \hat{n}_j \rangle$ , respectively. The parameters and configuration are the same as in SubsubSec. VD 1 and Fig. 5.

In (a) of both figures, both species hop preferentially to the right. Fig. 6 shows a clear domain wall structure. In Fig. 7, the cumulant is nearly zero except near the center. This again indicates that the steady state has little nonlocal correlation and resembles a product state.

In (b), species  $\sigma = 1$  hops rightward and  $\sigma = 2$  leftward. Both figures show a complex landscape very different from (a). Notably, Fig. 7(b) shows nonzero cumulant even for distant sites  $i, j$ , indicating correlations over

distances of particle sequence  $L$ . This confirms that the steady state has strong nonlocal correlations and is far from a product state.

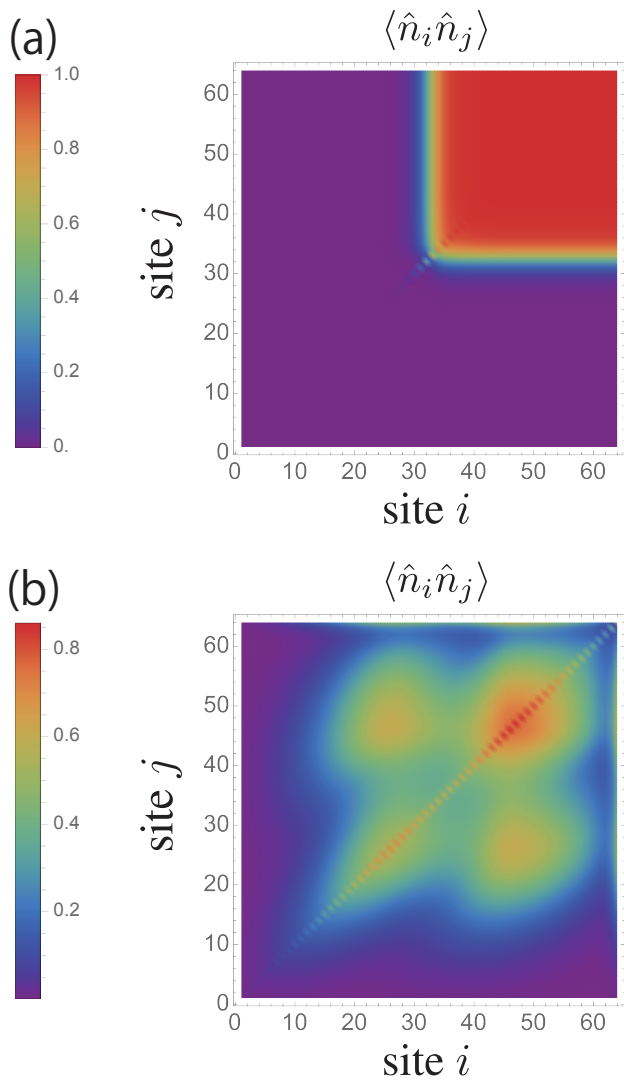


FIG. 6. Color plot of the particle number correlation function  $\langle \hat{n}_i \hat{n}_j \rangle$  with axes  $i$  and  $j$  for  $M = 2$ ,  $L = 64$ ,  $N = 32$ , and the configuration  $\{1,1,1,1,2,2,2,1,2,2,2,1,2,2,1,1,1,2,1,2,1,2,2,1,2,2,2,1,2,2,2,1\}$ . (a):  $(q_1, q_2) = (1.5, 1.25)$  case. Particles accumulate at the edges, forming a domain wall as in Fig. 5 and the ASEP steady state. (b):  $(q_1, q_2) = (1.5, 0.75)$  case. No clear domain wall appears, showing a behavior distinct from the standard ASEP's steady state.

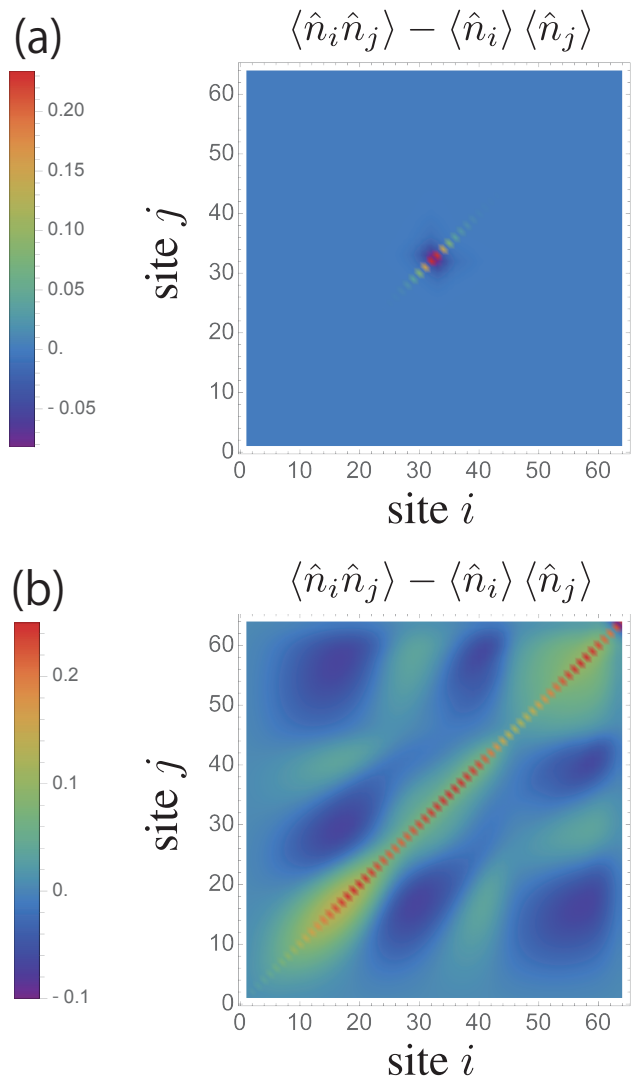


FIG. 7. Color plot of the cumulant of particle number correlation  $\langle \hat{n}_i \hat{n}_j \rangle - \langle \hat{n}_i \rangle \langle \hat{n}_j \rangle$  with axes  $i$  and  $j$  for  $M = 2$ ,  $L = 64$ ,  $N = 32$ , and the configuration  $\{1,1,1,1,2,2,2,1,2,2,2,1,2,2,1,1,1,2,1,2,1,2,1,2,2,1,2,2,2,1\}$ . (a):  $(q_1, q_2) = (1.5, 1.25)$  case. Non-zero values appear only near the center, indicating that the domain wall in Fig. 6 mainly arises from product densities. (b):  $(q_1, q_2) = (1.5, 0.75)$  case. The plot shows a complex landscape with long-range non-zero values, demonstrating nonlocal correlations in the steady state.

## VI. GAP STRUCTURE AND RELAXATION TIMES FOR TWO-SPECIES SYSTEM

In this section, we clarify how Hilbert space fragmentation explicitly leads to strong initial-state dependence of relaxation dynamics. Specifically, we study the spectral gap of  $H$  in the case of  $M = 2$ , as a proxy for the relaxation time  $\tau$  of the continuous-time Markov process generated by  $\tilde{H}$ . In each particle sequence sector  $\{\sigma\}_s$  of

the finite OBC system, we define the gap as

$$\Delta(\{\sigma\}_s) := E_1(\{\sigma\}_s) - E_0(\{\sigma\}_s), \quad (46)$$

where  $E_0(\{\sigma\}_s) = 0$  is the ground-state energy and  $E_1(\{\sigma\}_s)$  is the first excited-state energy. This definition includes possible edge modes that would vanish under periodic boundary conditions. Following Ref. [22], we note that in the many-body Markov processes the inverse relaxation time  $\tau(\{\sigma\}_s)^{-1}$  need not equal  $\Delta(\{\sigma\}_s)$  because superposition coefficients of steady state in real space basis can depend on system size. Here we use  $\Delta(\{\sigma\}_s)$  only as a rough estimate of  $\tau(\{\sigma\}_s)^{-1}$ . However, this rough estimate suggests that the relaxation dynamics are highly initial-state dependent due to Hilbert space fragmentation that severely restricts the dynamics in an initial-state-dependent manner. Indeed, even for the same parameters  $(p_1, p_2)$ , different initial states can lead either to rapid relaxation or the emergence of a metastable state.

### A. Smallest Gap Sector

By exact diagonalization, we find that the smallest gap across all sectors occurs in the one-hole sector  $N = L - 1$  with particle sequence

$$\left\{ \underbrace{1, \dots, 1}_{N_1}, \underbrace{2, \dots, 2}_{N_2} \right\}, \quad N_1 + N_2 = L - 1, \quad (47)$$

where  $N_1$  and  $N_2$  are chosen to minimize the gap. We denote this minimal gap by  $\Delta_{\min}$ . The restriction of  $H$  to this sector is an  $L \times L$  matrix given in Appendix E. Fig. 8 shows how  $\Delta_{\min}$  scales with  $L$  for parameters  $(p_1, p_2)$  (see Appendix D for numerical data).

In the region  $p_1 < \frac{1}{2}, p_2 < \frac{1}{2}$  or  $p_1 > \frac{1}{2}, p_2 > \frac{1}{2}$  (red in Fig. 8),  $\Delta_{\min}$  at  $L = 1024$  exceeds the threshold function  $G(L)$  defined in Ref. [23]:

$$\begin{aligned} G(L) &:= \frac{1 + a_L^2 b_L}{L - 1 + L^{3/2} a_L}, \\ a_L &:= -\frac{L - 1}{L^{3/2}} + \sqrt{\left(\frac{L - 1}{L^{3/2}}\right)^2 + \frac{1}{b_L}}, \\ b_L &:= \frac{6L^3}{(L - 1)(L - 2)(L - 3)}. \end{aligned} \quad (48)$$

OBC Knabe's method provides a lower bound on the spectral gap of a frustration-free infinite chain by comparing the finite-size gap to a threshold function  $G(L)$ . Concretely, the infinite-chain gap is bounded (up to a positive constant factor) by  $\Delta_{\min}(L) - G(L)$ . Hence, if exact diagonalization shows that  $\Delta_{\min}(L) - G(L) > 0$  at a finite  $L$ , one can conclude that the system retains an  $O(1)$  gap in the thermodynamic limit. Since  $G(L = 1024) = 0.000138884$  and  $\Delta_{\min}$  in all sample points satisfy  $\Delta_{\min} > G(1024)$ , Knabe's method for OBC proves a finite gap in this region (see Appendix C).

This agrees with the gapped Ising-like ferro XXZ line on  $p_1 = p_2$  (green) contained in the red region.

On the lines  $p_1 = \frac{1}{2}$  or  $p_2 = \frac{1}{2}$  (cyan),  $\Delta_{\min}$  closes as a power law,  $\Delta_{\min} \sim L^{-z}$  with  $z \geq 2$  (see Appendix D). This matches the bound  $z \geq 2$  for frustration-free gapless models [24, 25] and the Nambu–Goldstone magnon at  $p_1 = p_2 = \frac{1}{2}$  (Heisenberg limit).

In the region  $p_1 < \frac{1}{2} < p_2$  or  $p_2 < \frac{1}{2} < p_1$  (purple),  $\Delta_{\min}$  closes exponentially with  $L$  (see Appendix D) like Motzkin chain [26], Fredkin chain [27, 28] and others. This implies at least two degenerate steady states exist in the thermodynamic limit. This does not contradict the uniqueness of the ground state guaranteed by the Perron–Frobenius theorem, since that theorem applies only to finite-size matrices. For large but finite  $L$ , it indicates exponentially long relaxation times and metastable behavior. This phenomenon is absent in the ordinary OBC ASEP and is a unique feature of the no-passing ASEP in this parameter region.

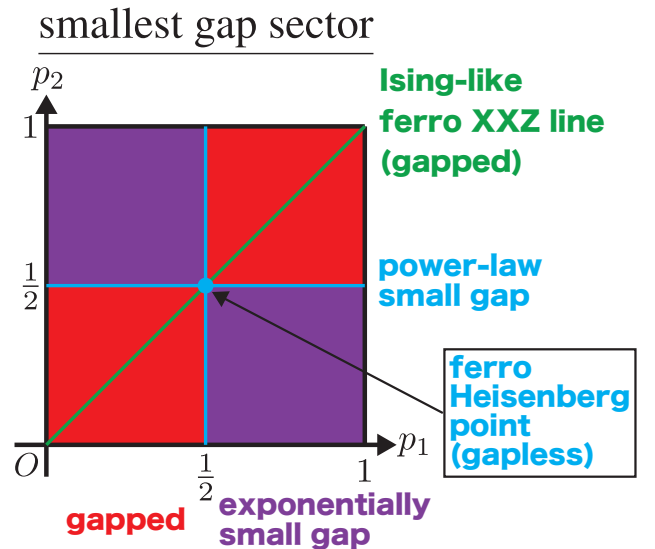


FIG. 8. Scaling of the minimal gap  $\Delta_{\min}$  with system size  $L$  in the sector with the minimal gap. In the red region ( $p_1 < \frac{1}{2}, p_2 < \frac{1}{2}$  or  $p_1 > \frac{1}{2}, p_2 > \frac{1}{2}$ ), Knabe's method [23] proves a finite gap. This region contains the Ising-like ferro XXZ line  $p_1 = p_2$  (green). On the cyan lines ( $p_1 = \frac{1}{2}$  or  $p_2 = \frac{1}{2}$ ), the gap closes as a power law with  $L$ . In the purple region ( $p_1 < \frac{1}{2} < p_2$  or  $p_2 < \frac{1}{2} < p_1$ ), the gap closes exponentially with  $L$ . The central point  $p_1 = p_2 = \frac{1}{2}$  is the gapless ferro Heisenberg limit.

### B. Single-Species XXZ Sector Gaps

Sectors with only one species  $\sigma$  reduce to the Ising-like ferro XXZ model (see Appendix. A). These sectors further decompose by total particle number  $\hat{N}$ . According to Ref. [21], under kink-boundary conditions, each sub-sector's gap is bounded below by the single-particle

gap

$$\Delta(\{\sigma\}) = 1 - 2\sqrt{p_\sigma(1-p_\sigma)} \cos\left(\frac{\pi}{L}\right) \xrightarrow{L \rightarrow \infty} 1 - 2\sqrt{p_\sigma(1-p_\sigma)}. \quad (49)$$

Thus for  $p_\sigma \neq \frac{1}{2}$ , all single-species sectors are gapped (red in Fig. 9). This is consistent with the result of SubSec. VIA. At  $p_\sigma = \frac{1}{2}$  (cyan), the Heisenberg limit is gapless. Fig. 9 illustrates this behavior for  $\sigma = 1$  and  $\sigma = 2$ .

### Ising-like ferro XXZ sector

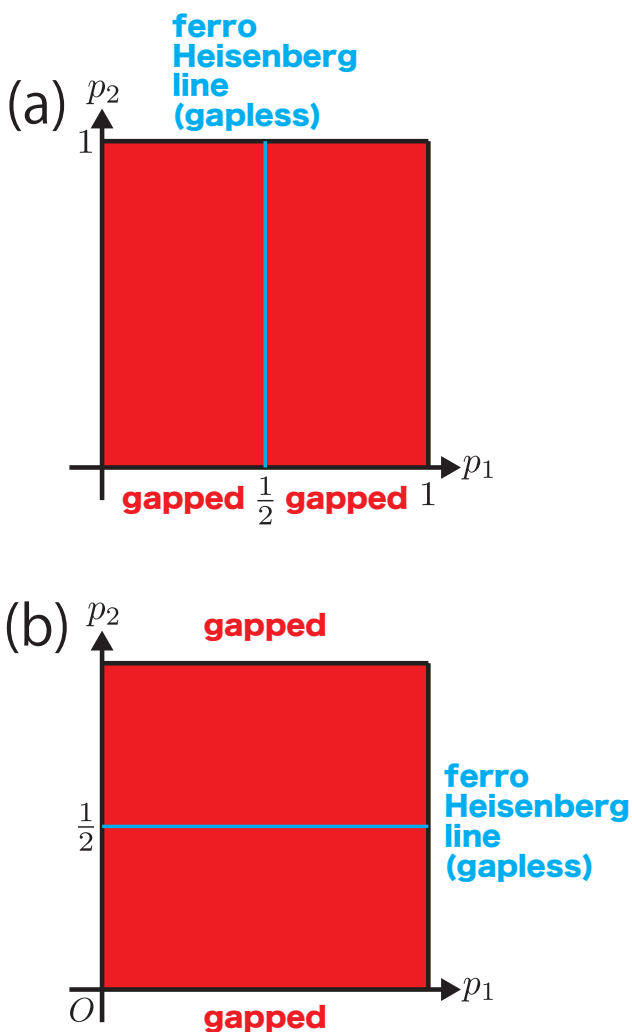


FIG. 9. Gaps in single-species sectors from (A1) or (A2). (a): Only species  $\sigma = 1$ . The gap is finite for  $p_1 \neq \frac{1}{2}$  and closes only at  $p_1 = \frac{1}{2}$ . (b): Only species  $\sigma = 2$ . The gap is finite for  $p_2 \neq \frac{1}{2}$  and closes only at  $p_2 = \frac{1}{2}$ .

### C. Global Gap Structure and Initial-State Dependence

Combining the results of Subsecs. VIA and VIB, we outline the gap structure in all sectors and discuss the strong initial-state dependence of the relaxation dynamics.

For instance, sectors with exponential gap closing can trap the system in metastable states for exponentially long times, significantly deviating from typical ASEP's behavior. Conversely, in sectors with a finite gap, relaxation occurs rapidly.

In the red region of Fig. 8, the lowest gap  $\Delta_{\min}$  remains  $O(1)$  as  $L \rightarrow \infty$ , and all sectors are gapped. In the purple region,  $\Delta_{\min}$  vanishes exponentially, so it does not bound other sectors. Although single-species XXZ sectors remain gapped there, some other sectors may be gapless. As a result of this, in the purple parameter region of Fig. 8, where the two species tend to hop in opposite directions, the relaxation behavior depends on the initial state, leading either to a finite relaxation time or to metastable dynamics. However, in the red parameter region of Fig. 8, where the two particle species tend to hop in the same direction, all particle sequence sectors exhibit a finite relaxation time and relax with little dependence on the initial state.

Since the purple parameter region of Fig. 8 also shows strong long-range correlations in the steady state (see SubSec. VD), determining gaps in each sector is an important open problem. In this frustration-free one-dimensional system, spontaneous breaking of  $U(1)$  symmetry and emergent Nambu–Goldstone modes may also cause gapless behavior [29]. Variational bounds with min-max principle, *nonrelativistic* field-theory approaches [24, 25], and the study of bulk gaps that exclude edge modes are promising directions for future work.

### VII. CONCLUSION

In this work, we introduced a multi-species no-passing ASEP on a one-dimensional open chain, to investigate how congestion phenomena that are rarely seen under periodic boundary conditions develop under the complex competition of hopping parameters. Our exact analytical and numerical analysis demonstrated how Hilbert space fragmentation directly leads to novel initial-state dependent dynamics and metastability absent in standard ASEP, as discussed in detail in Sec. VI and illustrated through particle distributions and correlation functions in Sec. VD.

Focusing on the two-species case, we discovered that when both species hop preferentially in the same direction the system exhibits a familiar domain-wall steady state profile with only weak correlations. This behavior is much like the standard ASEP.

In contrast, in the regions in which the particles' preferred hopping directions alternate the steady state de-

velops a richly structured density landscape with strong long-range correlations (Sec. VD, Figs. 5, 6, 7), and our spectral-gap analysis (Sec. VI, Fig. 8) revealed that some particle sequence sectors remain gapped—hence relax in  $O(1)$  time—while others become exponentially gapless. This novel sector-dependent gap structure explicitly gives rise to metastable relaxation dynamics absent in the usual exclusion processes.

Looking ahead, it will be important to establish rigorously the existence of a bulk gap in the thermodynamic limit by nonrelativistic field-theoretic methods and to quantify the degeneracy of steady states in each sector as  $L \rightarrow \infty$ . Inspired by the aquarium display of Razorfish that motivated our no-overtaking rule, one may generalize this framework to include some active-matter ingredients, thereby probing how fragmentation shapes collective migration. Kardar–Parisi–Zhang universality remains to be investigated like usual ASEP. Finally, treating the Hermitianized Hamiltonian  $H$  as a quantum chain opens the door to exploring the breakdown of eigenstate thermalization induced by Hilbert space fragmentation. We anticipate that these extensions will further illuminate the interplay between kinetic constraints, fragmentation, and nonequilibrium criticality in exclusion processes and beyond.

#### ACKNOWLEDGMENT

We would like to thank H. Katsura, M. Kunimi, T. Saito, T. Sasamoto, T. Takama, and K. Totsuka for their helpful discussions. This model was inspired by the display at AOA Sapporo Aquarium in Sapporo, Japan (<https://uu-nippon.com/hokkaido/corporate/aoao-sapporo.shtml>), which emphasized the mating behavior of Razorfish. We are especially grateful to AOA Sapporo Aquarium for showcasing Razorfish in such an innovative manner. U.M. was supported by JST SPRING, Grant Number JPMJSP2110, and JST CREST Grant Number JPMJCR19T2.

#### Appendix A: Sector Reducing to the Standard ASEP

Consider the sector containing particles of only a single species  $\tau$ . In this case, no interactions occur between different species, so the system reduces to the standard ASEP. After the similarity transformation, the Hermitian Hamiltonian (7) also reduces to the ferromagnetic XXZ model of the standard ASEP. Since  $b_{j,\sigma} = 0$  ( $\sigma \neq \tau$ ) and  $\hat{n}_j = \hat{n}_{j,\tau}$  in this sector, (5) and (7) for  $\tilde{H}$  and  $H$  reduce

to:

$$\begin{aligned} \tilde{H}^\tau &= \sum_{j=1}^{L-1} \tilde{h}_{j,j+1}^\tau, \\ \tilde{h}_{j,j+1}^\tau &= \\ & - \left[ p_\tau b_{j,\tau}^\dagger b_{j+1,\tau} + (1-p_\tau) b_{j+1,\tau}^\dagger b_{j,\tau} \right] \\ & + p_\tau (1 - \hat{n}_{j,\tau}) \hat{n}_{j+1,\tau} + (1-p_\tau) \hat{n}_{j,\tau} (1 - \hat{n}_{j+1,\tau}), \\ H^\tau &:= S \tilde{H}^\tau S^{-1} = \sum_{j=1}^{L-1} h_{j,j+1}^\tau, \\ h_{j,j+1}^\tau &= \\ & - \sqrt{p_\tau(1-p_\tau)} \left( b_{j,\tau}^\dagger b_{j+1,\tau} + b_{j+1,\tau}^\dagger b_{j,\tau} \right) \\ & + p_\tau (1 - \hat{n}_{j,\tau}) \hat{n}_{j+1,\tau} + (1-p_\tau) \hat{n}_{j,\tau} (1 - \hat{n}_{j+1,\tau}). \quad (\text{A1}) \end{aligned}$$

Here,  $\tilde{H}^\tau$  is the transition matrix of the standard ASEP. Its Hermitianized version is  $H^\tau$ . By identifying  $b_{j,\tau} = \sigma_j^-$  and  $b_{j,\tau}^\dagger = \sigma_j^+$ , with  $\sigma_j^\pm := \frac{1}{2}(\sigma_j^x \pm i\sigma_j^y)$  ( $\sigma^x, \sigma^y$  and  $\sigma^z$  are standard Pauli matrices with eigenvalues  $\pm 1$ ), we obtain a ferromagnetic XXZ model with kink-boundary condition [21]:

$$\begin{aligned} \tilde{h}_{j,j+1}^\tau &= \\ & - \frac{\sqrt{p_\tau(1-p_\tau)}}{2} (\sigma_j^x \sigma_{j+1}^x + \sigma_j^y \sigma_{j+1}^y) + \frac{1}{4} (1 - \sigma_j^z \sigma_{j+1}^z) \\ & - \frac{p_\tau - \frac{1}{2}}{2} (\sigma_j^z - \sigma_{j+1}^z). \quad (\text{A2}) \end{aligned}$$

This XXZ model is of Ising-like because  $0 < \sqrt{p_\tau(1-p_\tau)} \leq \frac{1}{2}$ . At  $p_\tau = \frac{1}{2}$ , the symmetric simple exclusion process case, it becomes the isotropic ferromagnetic Heisenberg model. This mapping to the XXZ model is important for dynamics and Hilbert space fragmentation [20], since the XXZ model is Bethe integrable and thus defines an integrable sector.

#### Appendix B: Algebraic Construction of ground states

In Sec. IV C, we constructed the MPS form of the ground states  $|\Psi_{\text{g.s.}}\rangle$  by heuristic arguments. Here we give an algebraic construction starting from the trivial vacuum  $|\Omega\rangle$  with  $H|\Omega\rangle = 0$ , using raising operators akin to a quantum group (cf. Appendix G of Ref. [30]).

We define  $M$  raising operators  $B_\sigma^\dagger$  ( $\sigma = 1, \dots, M$ ) by Ref. [30]:

$$B_\sigma^\dagger := \sum_{j=1}^L q_\sigma^j b_{j,\sigma}^\dagger, \quad (\text{B1})$$

$$= (1, 0) \begin{pmatrix} q_\sigma & b_{1,\sigma}^\dagger \\ 0 & 1 \end{pmatrix} \dots \begin{pmatrix} q_\sigma & b_{L,\sigma}^\dagger \\ 0 & 1 \end{pmatrix} \begin{pmatrix} 0 \\ 1 \end{pmatrix}. \quad (\text{B2})$$

One verifies

$$HB_\sigma^\dagger |\Omega\rangle = [H, B_\sigma^\dagger] |\Omega\rangle = 0, \quad (\text{B3})$$

$$[[H, B_{\sigma_1}^\dagger], B_{\sigma_2}^\dagger] = 0. \quad (\text{B4})$$

Because  $H$  is positive semidefinite and frustration-free, all ground states have energy zero. Let  $|\Psi_{\text{g.s.}}\rangle$  be any ground state so that  $H|\Psi_{\text{g.s.}}\rangle = 0$ . Then from (B4) we get

$$HB_{\sigma_1}^\dagger B_{\sigma_2}^\dagger |\Psi_{\text{g.s.}}\rangle = B_{\sigma_1}^\dagger HB_{\sigma_2}^\dagger |\Psi_{\text{g.s.}}\rangle + B_{\sigma_2}^\dagger HB_{\sigma_1}^\dagger |\Psi_{\text{g.s.}}\rangle. \quad (\text{B5})$$

Taking  $|\Psi_{\text{g.s.}}\rangle = |\Omega\rangle$  in (B5) and using (B3) gives

$$HB_{\sigma_1}^\dagger B_{\sigma_2}^\dagger |\Omega\rangle = 0 \quad (\forall \sigma_1, \sigma_2). \quad (\text{B6})$$

By iterating this argument, one shows

$$HB_{\sigma_1}^\dagger \cdots B_{\sigma_N}^\dagger |\Omega\rangle = 0 \quad (\forall \sigma_1, \dots, \sigma_N). \quad (\text{B7})$$

Hence any nonzero

$$B_{\sigma_1}^\dagger \cdots B_{\sigma_N}^\dagger |\Omega\rangle \quad (\text{B8})$$

is a ground state. We introduce the notation

$$|(r_1, \dots, r_M)\rangle := \left(B_1^\dagger\right)^{r_1} \cdots \left(B_M^\dagger\right)^{r_M} |\Omega\rangle, \quad (\text{B9})$$

with  $N = r_1 + \dots + r_M \leq L$ , which is nonzero ground state of  $H$  by the hard-core condition  $b_{j,\sigma_1}^\dagger b_{j,\sigma_2}^\dagger = 0$ .

To project onto a fixed particle sequence sector  $\{\sigma\}_s$  (an eigen sector of  $\mathcal{S}$ ), we use the MPO projection operators

$$\begin{aligned} & \hat{P}(\{\sigma\}_s) \\ &= \sum_{1 \leq j_1 < \dots < j_N \leq L} \left| 0, \dots, 0, \underset{j_1}{\sigma_1}, 0, \dots, 0, \underset{j_N}{\sigma_N}, 0, \dots, 0 \right\rangle \left\langle 0, \dots, 0, \underset{j_1}{\sigma_1}, 0, \dots, 0, \underset{j_N}{\sigma_N}, 0, \dots, 0 \right| \\ &= \mathbf{e}_1^\top \left( \begin{array}{ccc|ccc} |0\rangle\langle 0| & |\sigma_1\rangle\langle \sigma_1| & & & & \\ & |0\rangle\langle 0| & |\sigma_2\rangle\langle \sigma_2| & & & \\ & & & \ddots & & \\ & & & & |0\rangle\langle 0| & |\sigma_N\rangle\langle \sigma_N| \\ & & & & & |0\rangle\langle 0| \end{array} \right)_1 \cdots \left( \begin{array}{ccc|ccc} |0\rangle\langle 0| & |\sigma_1\rangle\langle \sigma_1| & & & & \\ & |0\rangle\langle 0| & |\sigma_2\rangle\langle \sigma_2| & & & \\ & & & \ddots & & \\ & & & & |0\rangle\langle 0| & |\sigma_N\rangle\langle \sigma_N| \\ & & & & & |0\rangle\langle 0| \end{array} \right)_L \mathbf{e}_{N+1} \\ &= \mathbf{e}_1^\top \left( \begin{array}{cccc} 1 - \hat{n}_1 & \hat{n}_{1,\sigma_1} & & \\ & 1 - \hat{n}_1 & \hat{n}_{1,\sigma_2} & \\ & & \ddots & \ddots \\ & & & 1 - \hat{n}_1 & \hat{n}_{1,\sigma_N} \\ & & & & 1 - \hat{n}_1 \end{array} \right) \cdots \left( \begin{array}{cccc} 1 - \hat{n}_L & \hat{n}_{L,\sigma_1} & & \\ & 1 - \hat{n}_L & \hat{n}_{L,\sigma_2} & \\ & & \ddots & \ddots \\ & & & 1 - \hat{n}_L & \hat{n}_{L,\sigma_N} \\ & & & & 1 - \hat{n}_L \end{array} \right) \mathbf{e}_{N+1}. \quad (\text{B10}) \end{aligned}$$

Applying projection  $\hat{P}(\{\sigma\}_s)$  to  $|(r_1, \dots, r_M)\rangle$  yields simultaneous eigenstates of  $H$  and  $\mathcal{S}$ .

Counting shows that for fixed  $N$ , there are

$$\sum_{r_1 + \dots + r_M = N} \frac{N!}{r_1! \cdots r_M!} = M^N \quad (\text{B11})$$

ground states, and summing  $N = 0, \dots, L$  gives  $\sum_{N=0}^L M^N = \frac{M^{L+1} - 1}{M - 1}$ , matching Sec. IV A.

Finally, by contracting zero singular-value bonds in the MPO form (B2) after projection, one recovers the MPS representation (30).

### Appendix C: Numerical Evidence for the Gap Existence

We apply OBC Knabe's method [23] for no-passing ASEP. In this method, each two-site term  $h_{j,j+1}$  in the

Hamiltonian  $H$  of (7) is a projector with eigenvalues 0 and 1. OBC Knabe's method states that if the gap at normalized system size  $L$  exceeds the threshold function  $G(L)$  in (48), then the model is rigorously gapped in the thermodynamic limit.

In Sec. VIA, we argued that the region with either  $p_1 < \frac{1}{2}$  and  $p_2 < \frac{1}{2}$ , or  $p_1 > \frac{1}{2}$  and  $p_2 > \frac{1}{2}$  (the red regions in Fig. 8), is gapped. By the parameter space symmetry of Sec. III B, it suffices to check the lower half of the yellow simplex in Fig. 3. We computed the minimal gap  $\Delta_{\min}$  by exact diagonalization at  $L = 1024$  for points on the boundary  $p_2 = 0.49$  with  $p_1 = 0.01, 0.02, \dots, 0.49$ . Fig. 10 compares these gaps to the threshold  $G(L = 1024) = 0.000138884$ . All computed gaps lie strictly above the threshold, confirming that these boundary points are gapped.

We also checked interior points of the red region by varying  $(p_1, p_2)$  from  $(0.01, 0.01)$  in steps of 0.01 at  $L = 1024$ . In every case, the computed  $\Delta_{\min}$  exceeded

$G(1024)$ , providing further numerical support that the entire red region is rigorously gapped.

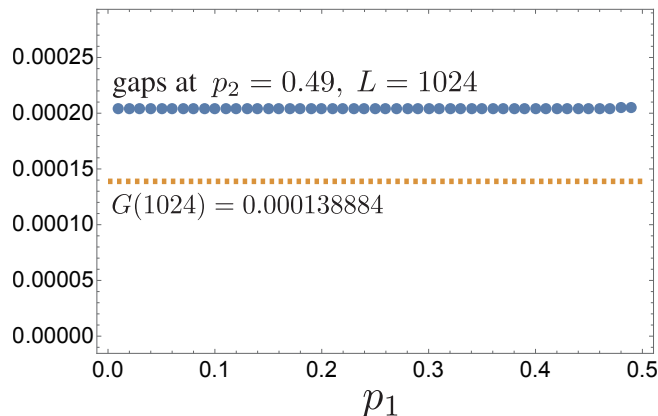


FIG. 10. Numerical verification of the gap using OBC Knabe's method [23]. Blue points show the minimal gap  $\Delta_{\min}$  at  $L = 1024$  for  $p_2 = 0.49$  and  $p_1 = 0.01, 0.02, \dots, 0.49$ . The orange dashed line marks the threshold  $G(1024) = 0.000138884$ . All gaps exceed the threshold, confirming these points are gapped.

#### Appendix D: Gap Closing Data for the Smallest Gap Sector

In Sec. VI A, we claimed that for  $p_1 = \frac{1}{2}$  or  $p_2 = \frac{1}{2}$  (the cyan lines in Fig. 8), the gap  $\Delta_{\min}$  closes algebraically with system size  $L$ . In contrast, for  $p_1 < \frac{1}{2} < p_2$  or  $p_2 < \frac{1}{2} < p_1$  (the purple regions in Fig. 8),  $\Delta_{\min}$  closes exponentially with system size  $L$ . Here we present numerical evidence supporting these behaviors.

Fig. 11 (a)–(c) show log–log plots of  $\Delta_{\min}$  versus  $L$  for  $(p_1, p_2) = (0.01, 0.5)$ ,  $(0.25, 0.5)$ , and  $(0.49, 0.5)$ , respectively. In all three cases, the data follow a power law and fits give dynamical critical exponents  $z = 2.015, 2.044$ , and  $2.320$ . These  $z \geq 2$  results are consistent with the result of Refs. [24, 25]. We also checked additional points with  $p_2 = \frac{1}{2}$  and  $p_1 = 0.01, 0.02, \dots, 0.49$ , and observed the same algebraic scaling.

Fig. 11 (d) is a semi–log plot of  $\Delta_{\min}$  versus  $L$  at  $(p_1, p_2) = (0.25, 0.75)$ . The linear trend confirms exponential gap closing. By using the symmetry of Sec. III B and sampling all points in the purple region in 0.01 increments as in Appendix C, we verified exponential gap closing throughout that purple region.

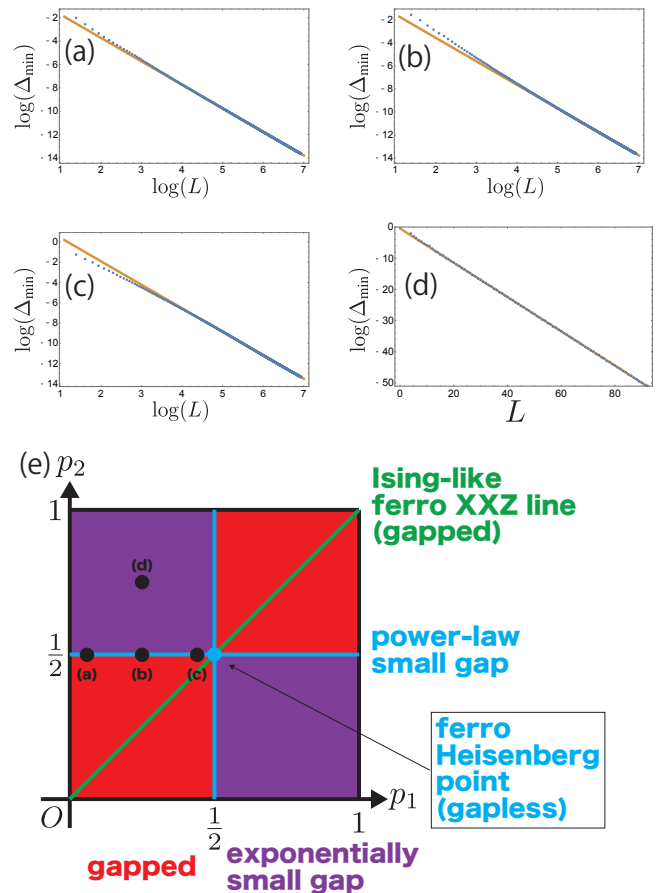


FIG. 11. Minimal gap  $\Delta_{\min}$  versus system size  $L$ . (a)–(c): Log–log plots at  $(p_1, p_2) = (0.01, 0.5)$ ,  $(0.25, 0.5)$ , and  $(0.49, 0.5)$ , showing algebraic gap closing with dynamical critical exponents  $z = 2.015, 2.044$ , and  $2.320$ . (d): Semi–log plot at  $(p_1, p_2) = (0.25, 0.75)$ , showing exponential gap closing. (e): Positions of these points in the parameter space from Fig. 8.

#### Appendix E: Matrix Representation of the Hamiltonian in the Smallest Gap Sector

We give here the matrix form of the Hamiltonian in the smallest gap sector used for numerical calculations in SubSec. VI A and Appendices C and D. In this sector, the basis is labeled solely by the position  $j$  of the hole





- 
- [1] Carolyn T MacDonald, Julian H Gibbs, and Allen C Pipkin. Kinetics of biopolymerization on nucleic acid templates. *Biopolymers: Original Research on Biomolecules*, 6(1):1–25, 1968. URL: <https://pubmed.ncbi.nlm.nih.gov/5641411/>.
- [2] Frank Spitzer. Interaction of Markov processes. *Advances in Mathematics*, 5(2):246–290, 1970. URL: <https://www.sciencedirect.com/science/article/pii/0001870870900344>, doi:10.1016/0001-8708(70)90034-4.
- [3] Thomas Milton Liggett. *Interacting particle systems*. Springer, 1985. URL: <https://link.springer.com/book/10.1007/b138374>.
- [4] Debashish Chowdhury, Ludger Santen, and Andreas Schadschneider. Statistical physics of vehicular traffic and some related systems. *Physics Reports*, 329(4):199–329, 2000. URL: <https://www.sciencedirect.com/science/article/pii/S0370157399001179>, doi:10.1016/S0370-1573(99)00117-9.
- [5] T Chou, K Mallick, and R K P Zia. Non-equilibrium statistical mechanics: from a paradigmatic model to biological transport. *Reports on Progress in Physics*, 74(11):116601, oct 2011. URL: <https://dx.doi.org/10.1088/0034-4885/74/11/116601>, doi:10.1088/0034-4885/74/11/116601.
- [6] B. Derrida. An exactly soluble non-equilibrium system: The asymmetric simple exclusion process. *Physics Reports*, 301(1):65–83, 1998. URL: <https://www.sciencedirect.com/science/article/pii/S0370157398000064>, doi:10.1016/S0370-1573(98)00006-4.
- [7] R A Blythe and M R Evans. Nonequilibrium steady states of matrix-product form: a solver’s guide. *Journal of Physics A: Mathematical and Theoretical*, 40(46):R333, oct 2007. URL: <https://dx.doi.org/10.1088/1751-8113/40/46/R01>, doi:10.1088/1751-8113/40/46/R01.
- [8] Alexei Borodin, Ivan Corwin, and Tomohiro Sasamoto. From duality to determinants for q-TASEP and ASEP. 2014. URL: <https://projecteuclid.org/journals/annals-of-probability/volume-42/issue-6/From-duality-to-determinants-for-q-TASEP-and-ASEP/10.1214/13-AOP868.full>.
- [9] Timothy Halpin-Healy and Yi-Cheng Zhang. Kinetic roughening phenomena, stochastic growth, directed polymers and all that. aspects of multidisciplinary statistical mechanics. *Physics Reports*, 254(4):215–414, 1995. URL: <https://www.sciencedirect.com/science/article/pii/037015739400087J>, doi:10.1016/0370-1573(94)00087-J.
- [10] M. R. Evans. Bose-Einstein condensation in disordered exclusion models and relation to traffic flow. *Europhysics Letters*, 36(1):13, oct 1996. URL: <https://dx.doi.org/10.1209/epl/i1996-00180-y>, doi:10.1209/epl/i1996-00180-y.
- [11] Attila Rákos and Gunter M Schütz. Bethe ansatz and current distribution for the TASEP with particle-dependent hopping rates. *Markov Processes And Related Fields*, 2005. URL: <https://math-mpfrf.org/journal/articles/id1083/>.
- [12] Masao Ogata and Hiroyuki Shiba. Bethe-ansatz wave function, momentum distribution, and spin correlation in the one-dimensional strongly correlated hubbard model. *Phys. Rev. B*, 41:2326–2338, Feb 1990. URL: <https://link.aps.org/doi/10.1103/PhysRevB.41.2326>, doi:10.1103/PhysRevB.41.2326.
- [13] Yves H. Kwan, Patrick H. Wilhelm, Sounak Biswas, and S. A. Parameswaran. Minimal Hubbard models of maximal Hilbert space fragmentation. *Phys. Rev. Lett.*, 134:010411, Jan 2025. URL: <https://link.aps.org/doi/10.1103/PhysRevLett.134.010411>, doi:10.1103/PhysRevLett.134.010411.
- [14] Tibor Rakovszky, Pablo Sala, Ruben Verresen, Michael Knap, and Frank Pollmann. Statistical localization: From strong fragmentation to strong edge modes. *Phys. Rev. B*, 101:125126, Mar 2020. URL: <https://link.aps.org/doi/10.1103/PhysRevB.101.125126>, doi:10.1103/PhysRevB.101.125126.
- [15] Pablo Sala, Tibor Rakovszky, Ruben Verresen, Michael Knap, and Frank Pollmann. Ergodicity breaking arising from Hilbert space fragmentation in dipole-conserving hamiltonians. *Phys. Rev. X*, 10:011047, Feb 2020. URL: <https://link.aps.org/doi/10.1103/PhysRevX.10.011047>, doi:10.1103/PhysRevX.10.011047.
- [16] Sanjay Moudgalya, B Andrei Bernevig, and Nicolas Regnault. Quantum many-body scars and Hilbert space fragmentation: a review of exact results. *Reports on Progress in Physics*, 85(8):086501, jul 2022. URL: <https://dx.doi.org/10.1088/1361-6633/ac73a0>, doi:10.1088/1361-6633/ac73a0.
- [17] Leh-Hun Gwa and Herbert Spohn. Bethe solution for the dynamical-scaling exponent of the noisy Burgers equation. *Phys. Rev. A*, 46:844–854, Jul 1992. URL: <https://link.aps.org/doi/10.1103/PhysRevA.46.844>, doi:10.1103/PhysRevA.46.844.
- [18] Naomichi Hatano and David R. Nelson. Localization transitions in non-Hermitian quantum mechanics. *Phys. Rev. Lett.*, 77:570–573, Jul 1996. URL: <https://link.aps.org/doi/10.1103/PhysRevLett.77.570>, doi:10.1103/PhysRevLett.77.570.
- [19] Naomichi Hatano and David R. Nelson. Vortex pinning and non-Hermitian quantum mechanics. *Phys. Rev. B*, 56:8651–8673, Oct 1997. URL: <https://link.aps.org/doi/10.1103/PhysRevB.56.8651>, doi:10.1103/PhysRevB.56.8651.
- [20] Urei Miura. To be published.
- [21] Tohru Koma and Bruno Nachtergaele. The spectral gap of the ferromagnetic XXZ-chain. *Letters in Mathematical Physics*, 40(1):1–16, 1997. URL: <https://link.springer.com/article/10.1023/A:1007351803403>.
- [22] David A Levin and Yuval Peres. *Markov chains and mixing times*, volume 107. American Mathematical Soc., 2017.
- [23] Marius Lemm and Evgeny Mozgunov. Spectral gaps of frustration-free spin systems with boundary. *Journal of Mathematical Physics*, 60(5), 2019. URL: <https://pubs.aip.org/aip/jmp/article/60/5/051901/234629/Spectral-gaps-of-frustration-free-spin-systems>.
- [24] Rintaro Masaoka, Tomohiro Soejima, and Haruki Watanabe. Quadratic dispersion relations in gapless frustration-free systems. *Phys. Rev. B*, 110:195140, Nov 2024.

- URL: <https://link.aps.org/doi/10.1103/PhysRevB.110.195140>, doi:10.1103/PhysRevB.110.195140.
- [25] Rintaro Masaoka, Tomohiro Soejima, and Haruki Watanabe. Rigorous lower bound of dynamic critical exponents in critical frustration-free systems, 2024. URL: <https://arxiv.org/abs/2406.06415>, arXiv:2406.06415.
- [26] Lionel Levine and Ramis Movassagh. The gap of the area-weighted Motzkin spin chain is exponentially small. *Journal of Physics A: Mathematical and Theoretical*, 50(25):255302, jun 2017. URL: <https://dx.doi.org/10.1088/1751-8121/aa6cc4>, doi:10.1088/1751-8121/aa6cc4.
- [27] Takuma Udagawa and Hosho Katsura. Finite-size gap, magnetization, and entanglement of deformed Fredkin spin chain. *Journal of Physics A: Mathematical and Theoretical*, 50(40):405002, sep 2017. URL: <https://dx.doi.org/10.1088/1751-8121/aa85b5>, doi:10.1088/1751-8121/aa85b5.
- [28] Zhao Zhang and Israel Klich. Entropy, gap and a multi-parameter deformation of the Fredkin spin chain. *Journal of Physics A: Mathematical and Theoretical*, 50(42):425201, sep 2017. URL: <https://dx.doi.org/10.1088/1751-8121/aa866e>, doi:10.1088/1751-8121/aa866e.
- [29] Haruki Watanabe, Hosho Katsura, and Jong Yeon Lee. Critical spontaneous breaking of U(1) symmetry at zero temperature in one dimension. *Phys. Rev. Lett.*, 133:176001, Oct 2024. URL: <https://link.aps.org/doi/10.1103/PhysRevLett.133.176001>, doi:10.1103/PhysRevLett.133.176001.
- [30] Jurriaan Wouters, Hosho Katsura, and Dirk Schuricht. Exact ground states for interacting Kitaev chains. *Phys. Rev. B*, 98:155119, Oct 2018. URL: <https://link.aps.org/doi/10.1103/PhysRevB.98.155119>, doi:10.1103/PhysRevB.98.155119.